ELSEVIER

Catalysis Today 50 (1999) 369–380

CATALYSIS TODAY

Decomposition of methanol on Pt-loaded ceria

Seiichiro Imamura[a,*], Takao Higashihara[a], Yoshio Saito[a], Hirofumi Aritani[a], Hiroyoshi Kanai[b], Yasuyuki Matsumura[c], Noritoshi Tsuda[d]

[a]*Faculty of Engineering and Design, Kyoto Institute of Technology, Matsugasaki, Sakyo-ku, Kyoto 606, Japan*
[b]*Department of Environmental Information, Kyoto Prefectural University, Shimogamo, Sakyo-ku, Kyoto 606, Japan*
[c]*Osaka National Research Institute, AIST, Midorigaoka, Ikeda, Osaka 563, Japan*
[d]*Faculty of Science and Engineering, Ritsumeikan University, 196 Noji-cho, Kusatsu, Shiga 525, Japan*

Abstract

Methanol was decomposed to carbon monoxide and hydrogen on supported precious metals. Among the precious metals examined the performance of Pt was found to be the best, and ceria was the best support. Pt/CeO_2 decomposed methanol completely at 230°C with 99.2% and 94.6% of selectivities to H_2 and CO, respectively. TEM, ESCA, and XAFS analyses showed that Pt interacted very strongly with ceria, indicating the possibility of the formation of Pt–O–Ce bond and the penetration of Pt into the bulk ceria. The reaction mechanism was discussed on the basis of the kinetic analysis.

Keywords: Methanol decomposition; Pt/CeO_2; State of Pt

1. Introduction

The decomposition of methanol to CO and H_2 (methanol reforming) is an important reaction because of its potential application in the technologies expected in the future. Methanol reforming can be applied in the fuel cell and used as an on-board reforming process for vehicle fuel. Advantage concerning energy transportation is also its merit: as liquids are more convenient for long-distance transportation than gases, methanol is conveyed to process sites, where it is converted into CO and H_2 and utilized for various purposes. Many catalysts for methanol decomposition have been developed [1–16]. Among them Ni and precious metals such as Pt or Pd seem to be effective, and the supports used are mainly Al_2O_3 and SiO_2. Although other supports such as TiO_2 and ZrO_2 are used, there does not seem to be so much data on CeO_2-supported catalysts. Li et al. investigated the action of CeO_2 in the decomposition of methanol; however, they only identified the adsorbed species of methanol on CeO_2 and no metal was supported on it [17]. On the other hand, CeO_2 is an inevitable component in the automobile catalysts; it stabilizes support alumina and keeps high surface area [18,19], prevents the sintering of precious metals, and thus, stabilizes their dispersed state [20,21], promotes CO oxidation [22–24] and water–gas shift reaction [25–27], and acts as an oxygen reservoir [28–37]. It can

*Corresponding author. Present address: Department of Chemistry, Kyoto Institute of Technology, Matsugasaki, Sakyo-ku, Kyoto 606, Japan. Tel.: +81-75-724-7534; fax: +81-75-724-7580; e-mail: imamura@ipc.kit.ac.jp

0920-5861/99/$ – see front matter
PII: S0920-5861(98)00516-1

also be used as a support for precious metals in the reactions other than the detoxification of vehicle exhaust gas: e.g. Pt–ceria for carbon monoxide hydrogenation [38], Rh–ceria for the decomposition of N_2O [39], and Ru–ceria for aqueous-phase or vapor-phase oxidation of formaldehyde [40,41]. As the superior action of ceria is often exclusively derived through the combination with precious metals, the knowledge on the interaction between ceria and precious metals is important to fully utilize the performance of both the elements in designing efficient catalysts. There seem to be discrepancies among the literature concerning the state of precious metals supported on ceria; that is, whether precious metals aggregate on the surface of ceria or interact with it and penetrate inside its bulk. Cook et al. reported that sintering of Pt on alumina is retarded by an addition of ceria at 600°C and 800°C and assume the strong interaction of Pt with Ce; however, Pt particles were observed by TEM [20]. Zafiris and Gorte [37] suggested the migration of Rh into ceria. Brogan et al. [42] reported the formation of a PtCeO complex on the basis of the analysis using Raman spectroscopy. Kalakkad et al. [38] observed the TEM image of Pt particles on any ceria supports which were used in the CO hydrogenation reaction. Zhou et al. suggested the migration of Rh into ceria to form a strong interaction with Ce^{3+} species. However, the extent of the interaction depends on the oxidation state of Ce, and Rh retains its metallic state on the surface when ceria is fully oxidized [43]. Bernal et al. [44] obtained clear TEM images of Rh metal particles on ceria. However, the recent fine review by Trovarelli [45] summarizes a considerable amount of data which demonstrates the strong interaction between precious metals with ceria with an atomic level.

In this work we first investigated the performance of Pt-loaded CeO_2 catalyst in the decomposition of methanol, and then, tried to clarify the state of Pt on CeO_2 by the combined use of XRD, TEM, ESCA, and XAFS techniques.

2. Experimental

2.1. Catalyst preparation

The supports (γ-Al_2O_3, ZrO_2, MgO, SiO_2/Al_2O_3, CaO), $H_2PtCl_6{\cdot}6H_2O$, $RhCl_3$, and $PdCl_2$ were used as obtained commercially. CeO_2 was prepared by precipitation from aqueous cerium(III) nitrate. One N NaOH was added to the solution until the pH became about 11. The resultant precipitate was washed with deionized water several times, and it was dried at 80°C overnight, followed by calcination at 500°C in air for 3 h. The BET surface areas of the supports were 81.0 m^2/g (CeO_2), 14.6 m^2/g (ZrO_2), 16.5 m^2/g (CaO), 198.2 m^2/g (γ-Al_2O_3), 46.3 m^2/g (MgO), and 188.0 m^2/g (SiO_2/Al_2O_3). Precious metals were loaded on the supports according to the two following methods. The first method employed the reduction of precious metals with formaldehyde. The supports were dispersed in an aqueous solution of precious metals maintained at 90°C, and aqueous formaldehyde (5 molar ratio to precious metal) was added to the solution. Then the pH of the solution was adjusted to about 9, and after the solution was stirred for 1 h, it was evaporated to dryness with an evaporator. The catalyst was dried at 80°C overnight and calcined at 500°C in air for 3 h. The second method employed the reduction with hydrogen. After an aqueous solution of precious metals dispersed with the supports was stirred for 1 h, it was evaporated to dryness. The catalysts thus obtained were reduced with hydrogen at 300°C for 1 h, followed by calcination at 500°C in air for 3 h. The catalysts prepared by the above two methods were pressed into a disk under a pressure of 30 MPa and was cut into 8–14 mesh size.

2.2. Apparatus and procedure

The decomposition of methanol was carried out with an ordinary tubular flow reactor under an atmospheric pressure. One milliliter of the catalyst was charged in the reactor and was reduced with hydrogen at 300°C for 1 h before the reaction. Argon containing 3.8 vol% of methanol was introduced into the reactor at a space velocity of 4200 h^{-1}. It was confirmed that the reactions were not affected by any mass transfer limitation inside the bulk catalyst because the conversion of methanol was independent of the catalyst particle size.

2.3. Analyses

Methanol was determined with a Shimadzu 4B gas chromatograph on a Porapack T column (2 m) at

140°C, and methane, CO, CO_2, and H_2 with a Shimadzu 3BT gas chromatograph on an activated charcoal column (1 m) at 60°C. The lattice constant of ceria was measured by an asymmetric photographing method using a Rigaku Denki Geigerflex D-3F equipped with a Debye–Scherrer camera. The radius of the camera was determined by the use of a silicon crystal powder as a standard. The 16 diffraction peaks of ceria observed by this method gave the averaged value of the lattice constant to a precision down to the third decimal place in Å unit. TEM and ESCA (XPS) analyses were carried out with a Hitachi H-800 transmission electron microscope and a Shimadzu ESCA 750 spectrophotometer, respectively. The binding energy (BE) of the ESCA peaks was calibrated on the basis of the BE of C_{1s} (285.0 eV) peak of the contaminated carbon species from the vacuum pump. The X-ray absorption spectra were obtained by a transmission mode at the beam line 10B station of the Photon Factory in the High Energy Accelerator Research Organization (Tsukuba) with a ring energy of 2.5 GeV and a ring current of 280–390 mA. A Si(3 1 1) double crystal was used to monochromatize the X-rays.

3. Results and discussion

3.1. Decomposition of methanol on Pt/CeO_2 and other catalysts

Table 1 shows the results of the decomposition of methanol on various catalysts. The temperature of the catalyst bed was increased at a rate of 2°C/min and the selectivities to CO and H_2 were obtained at a temperature of 100% methanol conversion. First, the activity of precious metals supported on a common support, CeO_2, was investigated. Among the catalysts in which precious metals were loaded on CeO_2 in the presence of formaldehyde, Rh/CeO_2 and Pt/CeO_2 had high activity as estimated by the temperatures of 50% and 100% methanol conversions (T_{50} and T_{100}) although the selectivity to CO was low on Rh/CeO_2. In the case of the catalysts prepared by the reduction with hydrogen, Pd/CeO_2, which showed the lowest activity when prepared by the formaldehyde method, exhibited high activity and comparatively high selectivity to H_2 and CO. Thus the performance of the catalysts remarkably depends on the method of preparation. Although the details of the effect of the

Table 1
Decomposition of methanol[a]

Catalyst[b]	Preparation method[c]	T_{50} (°C)[d]	T_{100} (°C)[e]	Selectivity (%)[f]	
				H_2	CO
Rh/CeO_2	A	183	230	92.6	63.7
Pt/CeO_2	A	192	230	99.2	94.6
Ru/CeO_2	A	221	270	89.0	41.6
Pd/CeO_2	A	223	280	87.1	67.9
Pd/CeO_2	B	174	220	100	86.6
Pt/CeO_2	B	158	240	100	91.1
Rh/CeO_2	B	193	270	88.3	68.5
Ru/CeO_2	B	217	280	88.2	74.0
Pt/ZrO_2	A	212	260	95.2	90.1
$Pt/\gamma\text{-}Al_2O_3$[g]	A	182	290	93.9	88.5
$Pt/SiO_2/Al_2O_3$[g]	A	218	320	94.0	88.7
Pt/CaO	A	253	320	100	75.3
Pt/MgO	A	290	380	39.2	69.9

[a]The reaction condition is shown in Section 2.
[b]Precious metal: 3 wt% loading.
[c]The catalysts were prepared by reduction with formaldehyde (A) and hydrogen (B) (see Section 2).
[d]Temperature of 50% methanol conversion.
[e]Temperature of complete methanol conversion.
[f]At T_{100}.
[g]A large amount of dimethyl ether was formed at low temperature region (around 190°C for $Pt/\gamma\text{-}Al_2O_3$ and 220°C for $Pt/SiO_2/Al_2O_3$).

catalyst preparation methods were unknown, we did not investigate this point further. As the activity and the selectivity were satisfactorily high for Pt/CeO_2 irrespective of the method of preparation, Pt was loaded on other supports by formaldehyde method in order to see the best support for Pt (see also Table 1). However, the performance of Pt loaded on other supports was far inferior to that of the Pt loaded on CeO_2; especially the temperatures of complete methanol decomposition were much higher except for Pt/ZrO_2. $Pt/\gamma\text{-}Al_2O_3$ and $Pt/SiO_2/Al_2O_3$ produced a large amount of dimethyl ether at a low temperature region probably due to the presence of acid sites [1]. As Pt/CeO_2 exhibited the highest performance with regard to both activity and selectivity, we investigate its action hereafter; the formaldehyde method was employed.

It was found that the activity of the catalyst increased linearly with an increase in the amount of Pt until 3 wt% of loading and thereafter became almost constant up to 5 wt% of Pt; the rate of methanol decomposition at 200°C was 1.5×10^{-3} mol/h g-cat for 0.5 wt% of Pt and 4.1×10^{-3} mol/h g-cat for 3 wt% loading. Fig. 1 shows the effect of the reaction temperature on the product distribution in the reaction over the catalyst with 1 wt% of Pt. The rate of methanol decomposition above 250°C (with complete methanol conversion) was 4.7×10^{-3} mol/h g-cat. The selectivities to CO and H_2 decreased with the temperature increase and methanation began to occur and CO_2 was formed simultaneously. CO_2 was probably formed by the reaction (shift reaction: Eq. (2)) of CO with H_2O which was formed through the methanation (Eq. (1)).

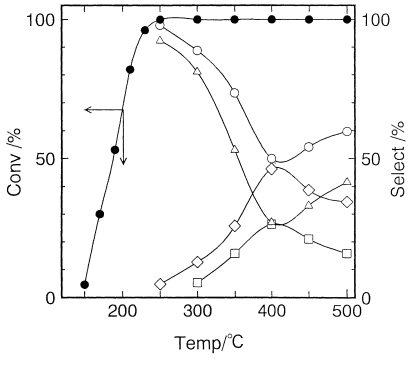

Fig. 1. Effect of the reaction temperature: (●) MeOH conversion; (○) H_2; (△) CO; (□) CO_2; (◇) CH_4. MeOH=3.8 vol% in Ar, Pt loading=1 wt%, SV=4200 h^{-1}.

$$CO + 3H_2 \rightleftarrows CH_4 + H_2O \quad (1)$$

$$CO + H_2O \rightleftarrows CO_2 + H_2 \quad (2)$$

The yields of CO_2 and CH_4 took maxima at 400°C and decreased above that temperature, and H_2 and CO again increased. As the shift reaction is slightly exothermic [46], high temperature runs reaction (2) backward, producing H_2O. Consequently, steam reforming of CH_4 (reverse reaction of Eq. (1)) would have occurred; steam reforming is endothermic and favors also high temperature [46]. It was found that a 100% conversion of methanol was maintained for 5 h at 250°C over the catalyst with 1 wt% of Pt, and selectivities to CO and H_2 did not change during that timescale. The change in the temperature (300–700°C) of the pretreatment of the catalyst (Pt: 1 wt%) with hydrogen did not affect its activity.

3.2. Kinetics of the decomposition of methanol

Kinetic study was performed to clarify the mechanism of methanol decomposition in the temperature region of 190–230°C. The conversion of methanol was maintained below 12% in order to satisfy the condition of a differential reactor. Methanol and hydrogen are dissociatively adsorbed on Pt easily [47–50], and CO is also chemisorbed on it [51,52]. Taking these adsorptions into consideration, following equilibria are obtained:

$$CH_3OH + 2Pt \rightleftarrows CH_3O{-}Pt + H{-}Pt, \quad K_m, \quad (3)$$

$$H_2 + 2Pt \rightleftarrows 2H{-}Pt, \quad K_h, \quad (4)$$

$$CO + Pt \rightleftarrows CO{-}Pt, \quad K_c. \quad (5)$$

The rate-determining step of methanol decomposition is assumed to be the abstraction of hydrogen atom from the methyl group since the reaction rate on Pt/SiO_2 decreases by substituting hydrogen atoms in the methyl group with deuteriums [53]. Thus we assume following reactions as the rate-determining steps:

$$CH_3O{-}Pt + H{-}Pt \rightarrow H_2CO{-}Pt + H_2 + Pt, \quad k_1, \quad (6)$$

$$CH_3O{-}Pt + Pt \rightarrow H_2CO{-}Pt + H{-}Pt, \quad k_2, \quad (7)$$

$$2CH_3O{-}Pt \rightarrow HCOOCH_3 + H_2 + 2Pt, \quad k_3, \quad (8)$$

$$CH_3O{-}Pt \rightarrow H_2CO{-}Pt + \tfrac{1}{2}H_2, \quad k_4. \quad (9)$$

Under the assumption that the partial pressures of CO and H_2 are small and that the species other than CH_3O–Pt are rapidly decomposed, we obtain rate expressions for each possible rate-determining step (Eqs. (6)–(9)) as follows, in which r represents the rate of methanol decomposition (see Appendix A for the example of the derivation of Eq. (10)).

For Eq. (6):

$$P_{\mathrm{MeOH}}^{1/2} r^{-1/2} = k_1^{-1/2} K_{\mathrm{m}}^{1/2} K_{\mathrm{h}}^{-1/2} P_{\mathrm{MeOH}} P_{\mathrm{H_2}}^{-1/2} + k_1^{-1/2} K_{\mathrm{m}}^{-1/2}. \quad (10)$$

For Eq. (7):

$$P_{\mathrm{MeOH}}^{1/2} P_{\mathrm{H_2}}^{-1/4} r^{-1/2} = k_2^{-1/2} K_{\mathrm{m}} K_{\mathrm{h}}^{-1/4} P_{\mathrm{MeOH}} P_{\mathrm{H_2}}^{-1/2} + k_2^{-1/2} K_{\mathrm{m}}^{-1/2} K_{\mathrm{h}}^{1/4}. \quad (11)$$

For Eq. (8):

$$P_{\mathrm{MeOH}} P_{\mathrm{H_2}}^{-1/2} r^{-1/2} = k_3^{-1/2} P_{\mathrm{MeOH}} P_{\mathrm{H_2}}^{-1/2} + k_3^{-1/2} K_{\mathrm{m}}^{-1} K_{\mathrm{h}}^{1/2}. \quad (12)$$

For Eq. (9):

$$P_{\mathrm{MeOH}} P_{\mathrm{H_2}}^{-1/2} r = k_4^{-1} P_{\mathrm{MeOH}} P_{\mathrm{H_2}}^{-1/2} + k_4^{-1} K_{\mathrm{m}}^{-1} K_{\mathrm{h}}^{1/2}. \quad (13)$$

Fig. 2 shows the plot of $P_{\mathrm{MeOH}} P_{\mathrm{H_2}}^{-1/2}$ vs. $P_{\mathrm{MeOH}}^{1/2} r^{-1/2}$ (Eq. (10)) and Fig. 3 $P_{\mathrm{MeOH}} P_{\mathrm{H_2}}^{-1/2}$ vs. $P_{\mathrm{MeOH}} P_{\mathrm{H_2}}^{-1/2} r^{-1/2}$ plot (Eq. (12)). Both plots show a fairly linear relationship. However, the plot for $P_{\mathrm{MeOH}} P_{\mathrm{H_2}}^{-1/2}$ vs. $P_{\mathrm{MeOH}}^{1/2} P_{\mathrm{H_2}}^{-1/4} r^{-1/2}$ (Eq. (11)) or that for $P_{\mathrm{MeOH}} P_{\mathrm{H_2}}^{-1/2}$ vs. $P_{\mathrm{MeOH}} P_{\mathrm{H_2}}^{-1/2} r$ (Eq. (13)) was not linear (not shown in the figure). Thus either Eq. (6) or Eq. (8) seems to be the rate-determining step. The slope of the straight line shown in Fig. 2 gave the value of $k_1^{-1/2} K_{\mathrm{m}}^{1/2} K_{\mathrm{h}}^{-1/2}$, the value of $k_1^{-1/2} K_{\mathrm{m}}^{-1/2}$ was obtained from the intercept on the ordinate. The Arrhenius plots of these values (190–230°C) gave a value of 53.4 kJ/mol for $E_{\mathrm{a}} + Q_{\mathrm{MeOH}} - Q_{\mathrm{H_2}}$ and 67.8 kJ/mol for $E_{\mathrm{a}} - Q_{\mathrm{MeOH}}$, where E_{a} is the activation energy for Eq. (6), and Q_{MeOH} and $Q_{\mathrm{H_2}}$ are the heats of dissociative adsorption of MeOH and H_2, respectively. Substitution of the reported value of $Q_{\mathrm{H_2}}$ (60–130 kJ/mol) on Pt gives the value of 91–126 kJ/mol for E_{a} and 23–58 kJ/mol for Q_{MeOH} [50]. The result is in accord with the fact that the heat of adsorption of methanol is considerably lower than that of hydrogen [54,55]. The same treatment for the data shown in Fig. 3 gives the

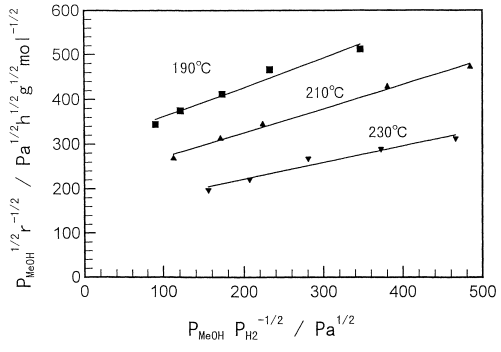

Fig. 2. Kinetic analysis – I. The reaction condition is the same as shown in Fig. 1.

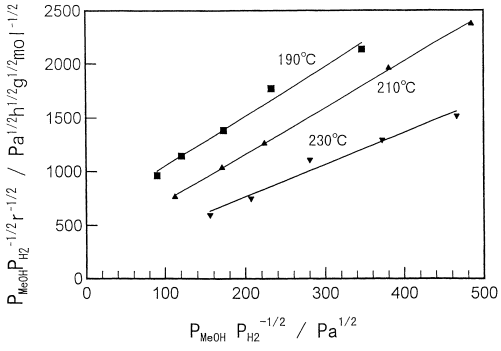

Fig. 3. Kinetic analysis – II.

values for $k_3^{-1/2}$ (slope) and $k_3^{-1/2} K_{\mathrm{MeOH}}^{-1} K_{\mathrm{h}}^{1/2}$ (intercept on ordinate), and the Arrhenius plots for these values give E_{a}=41.7 kJ/mol and $Q_{\mathrm{H_2}} - 2Q_{\mathrm{MeOH}}$= 79.5 kJ/mol. Thus we obtain −10 to 25 kJ/mol for Q_{MeOH}. The reported values for the heat of methanol adsorption on Pt(1 0 0) is ca. 50 kJ/mol [55]. Comparing this value with the values of Q_{MeOH} obtained in this work (23–58 kJ/mol for Eq. (6) and −10 to 25 kJ/mol for Eq. (8)), the plausible rate-limiting step is Eq. (6). The fact that the formation of methyl formate (Eq. (8)) was not observed during the reaction supports the above deduction.

The role of CeO_2 in the decomposition of methanol is not considered in the above discussion. Methanol is adsorbed on CeO_2 to produce methoxy and formate species, from which CO, H_2 or CO_2 may be produced [17]. This possibility cannot be neglected. However, the separate experiment showed that the rate of the methanol decomposition on pure CeO_2 was

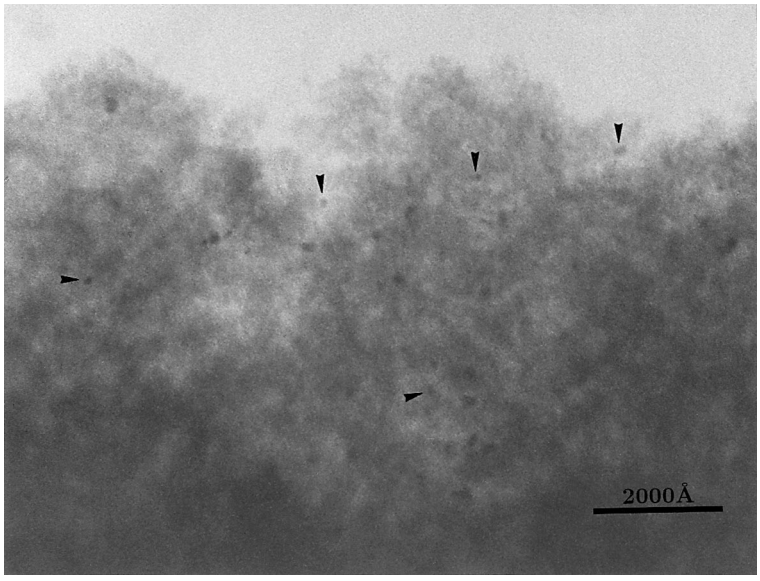

Fig. 4. TEM image of Pt(3 wt%)/γ-Al_2O_3. Arrows show the localized Pt.

3.3×10^{-4} mol/h g-cat at 200°C. This value is one order of magnitude smaller than those with Pt/CeO_2 catalysts. Thus the above discussion on the reaction mechanism, in which Pt plays as the main catalytic species, would be valid.

3.3. State of Pt on CeO_2

TEM observation was carried out for the catalysts which were prepared by formaldehyde method. The catalysts were pre-reduced in hydrogen at 400°C for 1 h (Pt: 3 wt%) in order to obtain a clear Pt image. Although Pt particles with a mean size of 100 Å were clearly observed on γ-Al_2O_3 (Fig. 4), no image of Pt was obtained on CeO_2 which was prepared by calcination at 500°C (Fig. 5). This situation is very much the same as that in the case of Rh supported on CeO_2, for which only the image of CeO_2 was observed [39]. When 1% of Pt was loaded on CeO_2 which was calcined at 950°C (BET surface area: 0.8 m^2/g), Pt particles were observed on very large CeO_2 crystals (Fig. 6). As the surface area of CeO_2 calcined at 500°C is large (81.0 m^2/g), one possibility is that Pt was too finely distributed to be detected by TEM. The other possibility is that Pt penetrated inside the CeO_2.

XRD patterns of Pt could not be obtained below 7 wt% Pt loading on CeO_2. Table 2 shows the change in the lattice constant (a_0) of CeO_2 on loading Pt by formaldehyde method. It was found that the CeO_2 calcined at 950°C had a value of a_0 of 5.412 Å which is in accordance with the literature value [56]; this CeO_2 seems to have a stoichiometric cubic structure. The a_0 of CeO_2 calcined at 500°C without Pt was 5.414(±0.002) Å, showing that crystallite formation is inadequate. On addition of Pt (1 and 3 wt%) and subsequent treatment with oxygen and hydrogen, the lattice constant increased to 5.421 Å. More rigorous treatment with 7 wt% of Pt and repeated oxidation–reduction cycles, a_0 further increased to 5.423 Å. This may indicate that Pt penetrated inside the CeO_2 and enlarged its lattice separation. However, the state of CeO_2 may be different in the presence and in the absence of Pt. In the presence of Pt, reduction of CeO_2 would be more remarkable, especially when treated with H_2, which would result in the lattice expansion because Ce^{3+} (1.03 Å) is larger than Ce^{4+} (0.92 Å). On the other hand, the loss of more lattice oxygen assisted by Pt would lead to the diminished lattice separation. In this respect, the change of the lattice constant would depend on the balance between these two factors. Therefore, the penetration of Pt into CeO_2 cannot be concluded on the basis of these XRD data.

The amount of Pt present in the surface layer of CeO_2 was measured with an ESCA spectrophotometer

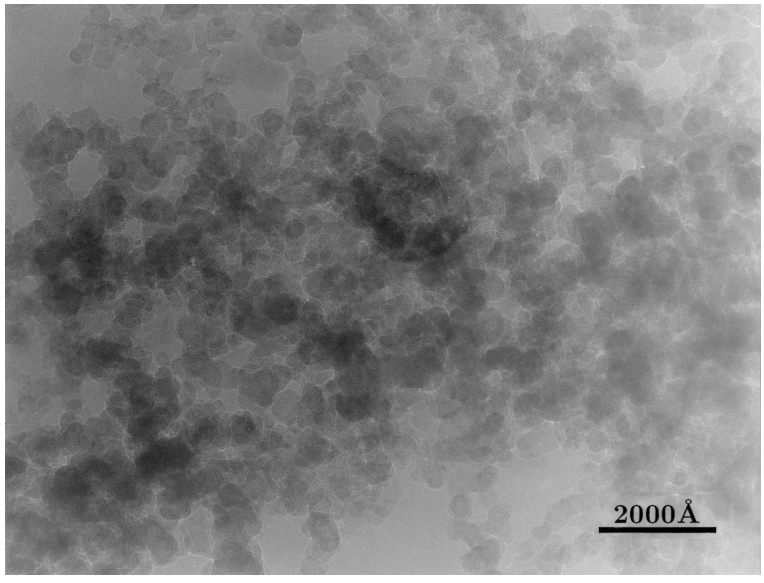

Fig. 5. TEM image of Pt(3 wt%)/CeO_2. CeO_2 was calcined at 500°C.

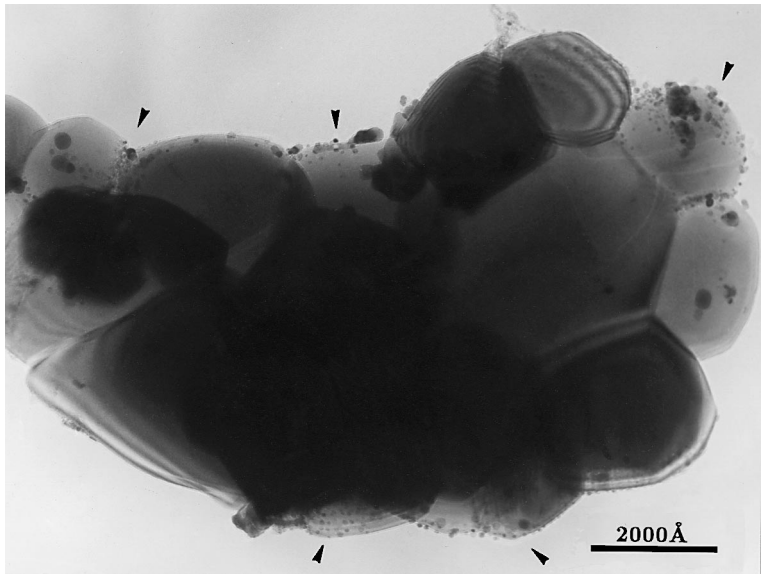

Fig. 6. TEM image of Pt(1 wt%)/CeO_2. CeO_2 was calcined at 950°C. Arrows show the localized Pt.

(Fig. 7). The samples were prepared in the same way as in the case of the TEM and XRD experiments. The Pt/Ce molar ratio was calculated on the basis of the ratio of the peak intensity of $4f_{5/2}$ plus $4f_{7/2}$ electrons for Pt to that of $4d_{3/2}$ plus $4d_{5/2}$ electrons for Ce. The surface Pt increased linearly with an increase in Pt loading; however, the surface Pt/Ce ratio was almost the same as that initially loaded. If the loaded Pt is present only on the surface, the surface Pt/Ce ratio should be higher than the loaded Pt/Ce ratio. When 1 wt% of Pt (Pt/Ce molar ratio of 0.009) was supported on CeO_2 which was calcined at 950°C, the

Table 2
Change in the lattice constant (a_0) of CeO_2

Sample	Treatment	a_0 (Å)[a]
CeO_2	500°C, 3 h, O_2	5.414±0.002
1 wt%Pt/CeO_2	500°C, 3 h, O_2+300°C, 1 h, H_2	5.421±0.001
3 wt%Pt/CeO_2	500°C, 3 h, O_2+300°C, 1 h, H_2	5.421±0.001
7 wt%Pt/CeO_2	500°C, 3 h, O_2+400°C, 1 h, H_2+400°C, 1 h, O_2+400°C, 1 h, H_2	5.423±0.001

[a]Average value obtained from 16 diffraction peaks of CeO_2.

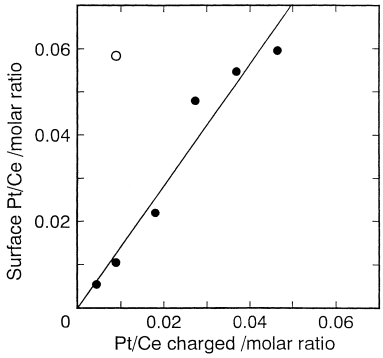

Fig. 7. ESCA analysis of the surface Pt concentration. Calcination temperature of CeO_2: (●) 500°C, (○) 950°C.

observed surface Pt/Ce ratio was much higher (0.058). Thus the result indicates the possibility of penetration of Pt into CeO_2 which has a large surface area due to the low calcination temperature of 500°C. Table 3 shows the result of Ar etching of Pt/CeO_2 (calcination temperature of CeO_2: 500°C, Pt loading: 3 wt%). The Pt/Ce molar ratio first decreased on 1 min Ar etching (estimated spattering depth of about 20 Å), and thereafter remains almost constant for 10 min. This also seems to indicate the dissolution of Pt into CeO_2. The

Table 3
ESCA analysis of Pt/CeO_2[a]

Ar etching (min)	Pt/Ce (molar ratio)	BE of $Pt_{4f_{7/2}}$ (eV)
0	0.0027	72.7
1	0.0021	74.5
3	0.0023	74.6
6	0.0027	74.5
10	0.0023	74.6

[a]CeO_2 was calcined at 500°C, and Pt was loaded by a formaldehyde method followed by reduction with hydrogen at 400°C. The amount of Pt loaded was 3 wt%, which corresponds to Pt/Ce molar ratio of 0.0026.

binding energy (BE) of the $4f_{7/2}$ electron of Pt was 72.65 eV before Ar etching and it increased to 74.5–74.64 eV after etching, which corresponds to the value for oxidized states of Pt such as PtO or PtO_2 [57]. The surface Pt was more reduced than its counterpart in the bulk; however, it was in more oxidized state than metallic Pt (71.2 eV).

The state of Pt was further investigated by an XAFS spectroscopy. Because of the large gradient of the background slope due to the existence of high concentration of CeO_2, Pt LIII-edge absorption could not be resolved clearly. Therefore, the samples with CeO_2 (5 wt%) and Pt (1 wt%) supported on γ-Al_2O_3 or SiO_2 were used for the XAFS measurement. After $Ce(NO_3)_3$ was impregnated on SiO_2 or Al_2O_3 and was calcined at 500°C, Pt was loaded on this CeO_2-supported SiO_2 or γ-Al_2O_3 by the usual formaldehyde method, followed by calcination at 500°C in air for 3 h. In the case of Pt–CeO_2 supported on Al_2O_3, incorporation of CeO_2 did not result in the activity increase of Pt; Pt seemed to contact mainly with Al_2O_3 although details are not known. On the other hand, CeO_2 on Pt/SiO_2 exhibited a promoting effect. The rate of methanol decomposition was 1.3×10^{-3} mol/h g-cat at 182°C over Pt(1 wt%)/CeO_2(5 wt%)/SiO_2, which can be compared with the reaction temperature of 263°C for the same rate over Pt(1 wt%)/SiO_2, suggesting the presence of an interaction between Pt and CeO_2. Thus, we analyzed the structure of Pt/CeO_2/SiO_2 sample by means of Pt LIII-edge XAFS. The XANES spectra of Pt(1 wt%)/SiO_2 and Pt(1 wt%)/CeO_2(5 wt%)/SiO_2 are shown in Fig. 8, together with those of the reference samples, PtO_2 (Pt^{4+}) and Pt foil (Pt^0). Because of the poor resolution in those spectra, the absorption-edge energy of PtO_2 was almost the same as that of Pt foil. The difference is that the sharp and intense white line is observed in PtO_2 compared with Pt foil. The intensity of this white

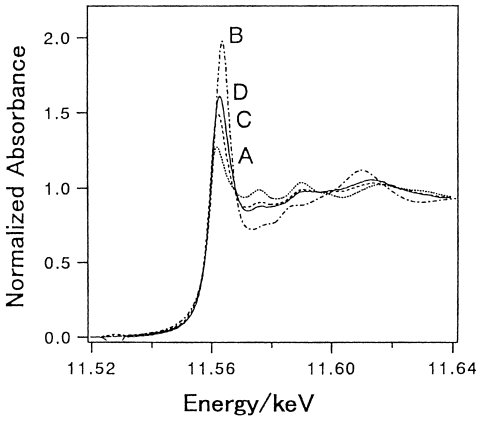

Fig. 8. Pt-LIII edge XANES: (A) Pt foil, (B) PtO_2, (C) Pt(1 wt%)/SiO_2, and (D) Pt(1 wt%)/CeO_2(5 wt%)/SiO_2.

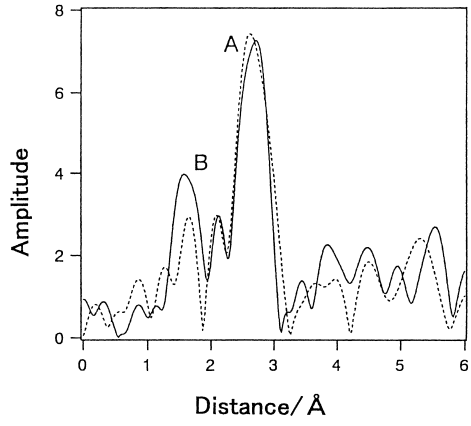

Fig. 10. Fourier transformed EXAFS of (A) Pt(1 wt%)/SiO_2 and (B) Pt(1 wt%)/CeO_2(5 wt%)/SiO_2.

line reflects unoccupancy of Pt 5d orbitals, because Pt L-edge XANES is mainly caused by the electron transition from 2p to 5d orbitals of the Pt atom. Thus its intensity is related to the oxidation state of Pt atom [58–60]. The intensity of the white line is higher for Pt(1 wt%)/SiO_2 than for Pt foil, indicating that some part of Pt atom exists in oxidized states. For Pt(1 wt%)/CeO_2(5 wt%)/SiO_2, the white line is even higher. Thus, the Pt atom is present in a more oxidized state in the presence of CeO_2 on SiO_2-support.

Fig. 9 shows the Fourier transform (k^3-weighted) EXAFS of Pt foil and PtO_2 without any phase-shift correction. Pt–O scattering on PtO_2 appears at the position of 1.6 Å, and Pt–Pt scattering at 2.9 Å. For Pt foil, a peak due to Pt–Pt is seen at 2.6 Å. In addition, a peak at 2.1 Å can be seen, which is caused both by the k-dependent behavior of back-scattering amplitude and non-linearity in the phase-shift function [61]. Fig. 10 shows the FT results for Pt(1 wt%)/SiO_2 and Pt(1 wt%)/CeO_2(5 wt%)/SiO_2. In the case of Pt(1 wt%)/SiO_2, two peaks appeared due to Pt–O (at 1.6 Å) and metallic Pt–Pt (2.6 Å) scatterings. This result, together with the result of the XANES analysis, suggests that the Pt is present as a mixture of Pt^0 and oxidized Pt ion. Relative FT magnitude of Pt–O peak increased when CeO_2 was introduced. This implies the increase in the oxidized state of Pt, which is in accordance with the result of the XANES analysis. Although a slight change is seen in the second shell region, this difference is within an analytical error. In order to clarify the difference in the local structure, curve-fitting analysis was introduced and the result is shown in Table 4. The method of data analysis is described elsewhere [62–64]. Back-scattering amplitudes for oxygen and platinum atoms were extracted from FTs of PtO_2 and Pt foil. For Pt(1 wt%)/SiO_2, metallic Pt–Pt scattering can be fitted by one-shell model, where R=2.77 Å and coordination number (CN)=8.5; metallic Pt cluster exists as a micro-particle because the CN is lower than that of Pt metal (R=2.77 Å and CN=12). In the case of Pt(1 wt%)/CeO_2(5 wt%)/SiO_2, two-shell fitting of Pt–Pt shells was the best method to estimate the parameters, R and CN. In this case, one shell had R=2.70 Å and CN=2.3, and the other R=2.81 Å and CN=3.2. It should be noted that the total CN of Pt(1 wt%)/CeO_2(5 wt%)/

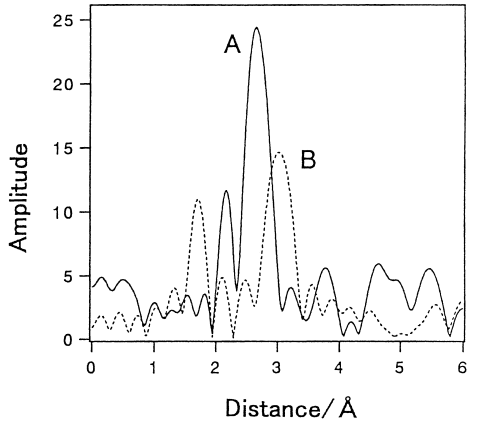

Fig. 9. Fourier transformed EXAFS of Pt foil (A) and PtO_2 (B).

Table 4
Structural parameters for Pt(1 wt%)/CeO_2 and Pt(1 wt%)/CeO_2(5 wt%)/SiO_2

		R (Å)	CN[a]	Debye–Waller (pm^2)
Pt(1 wt%)/SiO_2	Pt–O	1.98	2.7	32
	Pt–Pt	2.77	8.5	34
Pt(1 wt%)CeO_2(5 wt%)/SiO_2	Pt–O	1.97	3.1	36
	Pt–Pt	2.70	2.3	−21
	Pt–Pt	2.81	3.2	−20

[a]Coordination number.

SiO_2 is smaller than that of Pt(1 wt%)/SiO_2, suggesting that the component of metallic Pt species is limited and Pt exists as smaller particles such as oligomers. This result together with the result of XANES analysis shows that Pt atom in Pt(1 wt%)/CeO_2(5 wt%)/SiO_2 exists partly as an extremely small metal particle, whose local structure is different from the metallic Pt on SiO_2 because of the coexistence of CeO_2. Oxidized state of Pt is also stabilized.

The TEM image of Pt could not be obtained on the ceria with a large surface area (81.0 m^2/g), while Pt particle was clearly seen to exist when its surface area of ceria was large (0.8 m^2/g). Thus Pt and ceria strongly interact when the surface of ceria is active (large surface area). The result of the surface Pt concentration measurement (ESCA) indicates the possibility of the dissolution of Pt into the bulk ceria. If dissolution of Pt into CeO_2 lattice occurs, Pt must be in the oxidized state because Pt^0 is too large to replace Ce^{4+} or Ce^{3+} (ionic radii: Pt^{2+} 0.86 Å, Pt^{4+} 0.70, Ce^{3+} 1.03 Å, Ce^{4+} 0.92 Å, and atomic radius of Pt metal 1.38 Å) [65]. XAFS analysis indicated that the incorporation of ceria resulted in the particle size decrease of Pt metal and simultaneous increase in the oxidation state of Pt. Thus it is reasonably supposed that Pt–O–Ce interaction exists, which is in accord with the observation by TEM and ESCA analyses and may support the dissolution of Pt into bulk ceria. The real state of Pt on the surface is difficult to deduce. Pt would be present as very fine particles (even as oligomers). In that case, oxidized state of Pt exists in the interface region between Pt particles (oligomers) and ceria in the form of Pt–O–Ce. The result of methanol decomposition demonstrates that the dispersed state of Pt is highly efficient in activating CO or H_2. The rate-determining step was assumed to be the abstraction of methoxy hydrogen bound to Pt (Eq. (6)). When Pt takes an oxidized state in the presence of ceria, electron is withdrawn from the methoxy group to Pt and C–H bond of the methoxy group will be weakened, resulting in the acceleration of the reaction. It is also reported that, in the decomposition of methanol over Pd catalyst, the oxidized state of Pd is more active than zero-valent Pd [66].

Acknowledgements

This work was performed under the approval of the Photon Factory Program Advisory Committee of High Energy Research Organization (Proposal no. 96G169). The authors thank Prof. M. Nomura and Mr. A. Koyama of KEK-PF of Tsukuba, for the X-ray measurement. The encouragement by Dr. T. Tanaka of Kyoto University is acknowledged. The authors also thank Mr. K. Utani of Kyoto Institute of Technology for his kind cooperation.

Appendix A

The following equilibria are derived from Eqs. (3)–(6):

$$K_m = (\theta_{CH_3O}\theta_H)/(P_{MeOH}\theta_S^2),$$
$$K_h = \theta_H^2/(P_{H_2}\theta_S^2), \quad K_c = \theta_{CO}/(P_{CO}\theta_S),$$

where θ_{CH_3O}, θ_H, θ_{CO}, and θ_S are the concentrations of CH_3–Pt, H–Pt, CO–Pt and the vacant sites of Pt, respectively. From the above equations we obtain

$$\theta_H = K_h^{1/2}P_{H_2}^{1/2}\theta_S, \quad \theta_{CO} = K_cP_{CO}\theta_S,$$
$$\theta_{CH_3O} = K_mP_{MeOH}\theta_S^2/\theta_H = K_mP_{MeOH}\theta_S^2/K_h^{1/2}P_{H_2}^{1/2}\theta_S$$
$$= K_mK_h^{-1/2}P_{MeOH}P_{H_2}^{-1/2}\theta_S.$$

Using the condition, $\theta_S + \theta_{CH_3O} + \theta_H + \theta_{CO} = 1$, θ_S is expressed as

$$\theta_S = 1/(1+K_m K_h^{-1/2} P_{MeOH} P_{H_2}^{-1/2} + K_h^{1/2} P_{H_2}^{1/2} + K_c P_{CO}).$$

Then the rate of Eq. (6) is expressed by

$$r = k_1 \theta_{CH_3O} \theta_H = k_1 K_m P_{MeOH} \theta_S^2$$
$$= k_1 K_m P_{MeOH} / (1 + K_m K_h^{-1/2} P_{MeOH} P_{H_2}^{-1/2} + K_h^{1/2} P_{H_2}^{1/2} + K_c P_{CO})^2.$$

From the above equation, Eq. (10) was derived on the assumption that P_{H_2} and P_{CO} are negligibly small.

$$P_{MeOH}^{1/2} r^{-1/2} = k_1^{-1/2} K_m^{1/2} K_h^{-1/2} P_{MeOH} P_{H_2}^{-1/2} + k_1^{-1/2} K_m^{-1/2}. \quad (10)$$

References

[1] H. Niiyama, S. Tamai, J.S. Kim, E. Echigoya, Sekiyu Gakkaishi 42 (1981) 322.
[2] M. Suehiro, Y. Nagaki, T. Inui, Y. Takegami, Sekiyu Gakkaishi 26 (1983) 150.
[3] N. Kruse, G.K. Chuah, G. Abend, D.L. Cocke, J.H. Block, Surf. Sci. 189 190 (1987) 832.
[4] J.N. Russell Jr., I. Chorkendorff, I.T. Yates Jr., , Surf. Sci. 183 (1987) 316.
[5] M. Akiyoshi, H. Hattori, K. Tabnabe, Sekiyu Gakkaishi 30 (1987) 156.
[6] M. Akiyoshi, H. Hattori, Sekiyu Gakkaishi 31 (1988) 239.
[7] O. Tokunaga, Y. Satoh, T. Fukushima, S. Ogasawara, Sekiyu Gakkaishi 33 (1990) 173.
[8] Y. Saitoh, S. Ohtsu, Y. Makie, T. Okada, K. Satoh, N. Tsuruta, Y. Terunuma, Bull. Chem. Soc. Jpn. 63 (1990) 108.
[9] H. Imamura, T. Takada, S. Kasahara, S. Tsuchiya, Appl. Catal. 58 (1990) 165.
[10] X. Jiang, J.E. Parmeter, C.A. Estrada, D.W. Goodman, Surf. Sci. 249 (1991) 44.
[11] J. Wang, R.I. Masel, Surf. Sci. 243 (1991) 199.
[12] J. Wang, R.I. Masel, J. Am. Chem. Soc. 113 (1991) 5850.
[13] D.T. Wickham, B.W. Logsdon, S.W. Cowley, C.D. Bulter, J. Catal. 128 (1991) 198.
[14] J. Rasko, J. Bontovics, F. Solymosi, J. Catal. 146 (1994) 22.
[15] C. Fukuhara, N. Sasahara, A. Igarashi, Sekiyu Gakkaishi 37 (1994) 173.
[16] C. Fukuhara, S. Sekiguchi, H. Muto, A. Igarashi, Kagaku Kogaku Ronbunshu 21 (1995) 1002.
[17] C. Li, K. Domen, K. Maruyama, T. Onishi, J. Catal. 125 (1990) 445.
[18] B. Harrison, A.F. Diwell, C. Hallett, Plat. Met. Rev. 32 (1988) 73.
[19] M. Ozawa, M. Kimura, J. Mater. Sci. Lett. 9 (1990) 291.
[20] A. Cook, A.G. Fitzgerald, J.A. Cairns, in: T.J. Dines, C.H. Rochester, J. Thomson (Eds.), Catalysis and Surface Characterization, Royal Society of Chemistry, Cambridge, 1992, p. 249.
[21] F.L. Normand, L. Hilaire, K. Kili, G. Maire, J. Phys. Chem. 92 (1988) 2561.
[22] Y.F. Yu Yao, J. Catal. 87 (1984) 152.
[23] J.G. Numan, H.J. Robota, M.J. Cohn, S.A. Bradley, J. Catal. 133 (1992) 309.
[24] C. Serre, F. Garin, G. Belot, G. Maire, J. Catal. 141 (1993) 1.
[25] J.C. Schlatter, P.J. Mitchell, Ind. Eng. Chem. Prod. Res. Dev. 19 (1980) 288.
[26] G. Kim, Ind. Eng. Chem. Prod. Res. Dev. 21 (1982) 267.
[27] E.C. Su, W.G. Rothschild, J. Catal. 99 (1986) 506.
[28] S. Imamura, M. Shono, N. Okamoto, A. Hamada, S. Ishida, Appl. Catal. A 142 (1996) 279.
[29] H.C. Yao, Y.F. Yu Yao, J. Catal. 86 (1984) 254.
[30] E.C. Su, C.N. Montreuil, W.W. Rothschild, Appl. Catal. 17 (1985) 75.
[31] B.H. Engler, E. Koberstein, P. Schubert, Appl. Catal. 48 (1989) 71.
[32] P. Loof, B. Kasemo, K.E. Keck, J. Catal. 118 (1989) 339.
[33] T. Miki, T. Ogawa, M. Haneda, N. Kakuta, A. Ueno, S. Tateishi, S. Matsuura, M. Sato, J. Phys. Chem. 94 (1990) 339.
[34] C. Padeste, N.W. Cant, D. L Trimm, Catal. Lett. 18 (1993) 305.
[35] S. Kacimi, J. Barbier Jr., R. Taha, D. Duprez, Catal. Lett. 22 (1993) 343.
[36] G.S. Zafiris, R.J. Gorte, J. Catal. 143 (1993) 86.
[37] G.S. Zafiris, R.J. Gorte, J. Catal. 139 (1993) 561.
[38] D.S. Kalakkad, A.K. Datye, H.J. Robota, J. Catal. 148 (1994) 729.
[39] S. Imamura, N. Okamoto, Y. Saito, T. Ito, H. Jindai, J. Jpn. Petrol. Inst. 39 (1996) 350.
[40] S. Imamura, I. Fukuda, S. Ishida, Ind. Eng. Chem. Res. 27 (1988) 718.
[41] S. Imamura, D. Uchihori, K. Utani, T. Ito, Catal. Lett. 24 (1994) 377.
[42] M.S. Brogan, J.A. Cairns, T.J. Dines, in: T.J. Dines, C.H. Rochester, J. Thomson (Eds.), Catalysis and Surface Characterization, Royal Society of Chemistry, Cambridge, 1992, p. 282.
[43] T. Zhou, M. Nakashima, J.M. White, J. Phys. Chem. 92 (1988) 812.
[44] S. Bernal, F.J. Botana, J.J. Calvino, M.A. Cauqui, G.A. Cifredo, A. Jobacho, J.M. Pintado, J.M. Rodiguez-Izquierdo, J. Phys. Chem. 97 (1993) 4118.
[45] A. Trovarelli, Catal. Rev. 38 (1996) 439.
[46] G.A. Somorjai, in: Introduction to Surface Chemistry and Catalysis, Wiley, New York, 1994, p. 485.
[47] J. Wang, R.I. Masel, Surf. Sci. 243 (1991) 199.
[48] A.K. Bhattacharya, M.A. Chesters, M.E. Pemble, N. Sheppard, Surf. Sci. 206 (1988) L845.
[49] G.E. Gdowski, J.A. Fair, R.J. Madix, Surf. Sci. 127 (1983) 541.
[50] I. Toyoshima, G.A. Somorjai, Catal. Rev.-Sci. Eng. 19 (1979) 105.

[51] D.H. Ehlers, A.P. Esser, A. Spitzer, H. Lüth, Surf. Sci. 191 (1987) 466.
[52] C.T. Campbell, G. Ertl, H. Kuipers, J. Segner, Surf. Sci. 107 (1981) 207.
[53] O. Tokugawa, Y. Satoh, T. Fukushima, S. Ogasawara, Sekiyu Gakkaishi 33 (1990) 173.
[54] B.A. Sexton, Surf. Sci. 102 (1981) 271.
[55] B.A. Sexton, K.D. Rendulic, A.E. Hughes, Surf. Sci. 121 (1982) 181.
[56] J.V. Smith (Ed.), in: X-Ray Power Data File, Sets 1–5, American Society for Testing and Materials, Swarthmore, 1967, p. 534.
[57] D. Briggs, M. Seah (Eds.), in: Practical Surface Analysis, Auger and X-Ray Photoelectron Spectroscopy, vol. 1, 2nd ed., Wiley, New York, 1990, p. 621.
[58] J.A. Horsley, J. Chem. Phys. 76 (1982) 1451.
[59] J.C. Bart, Adv. Catal. 34 (1986) 270.
[60] S. Yoshida, T. Tanaka, in: Y. Iwasawa (Ed.), X-Ray Absorption Fine Structure for Catalysts and Surfaces, World Scientific, Singapore, 1996, p. 304.
[61] J.B.A.D. van Zon, D.C. Koningsberger, H.F.J. van't Bilk, R. Prins, J. Chem. Phys. 80 (1984) 3914.
[62] S. Yoshida, T. Tanaka, T. Hanada, T. Hiraiwa, H. Kanai, T. Funabiki, Catal. Lett. 12 (1992) 277.
[63] H. Kanai, H. Mizutani, T. Tanaka, T. Funabiki, S. Yoshida, M. Takano, J. Mater. Chem. 2 (1993) 703.
[64] T. Tanaka, H. Yamashita, R. Tsuchitani, T. Funabiki, S. Yoshida, J. Chem. Soc., Faraday Trans. 84 (1988) 2987.
[65] J.A. Dean (Ed.), in: Lange's Handbook of Chemistry, 13th ed., McGraw-Hill, New York, 1985 pp. 3–121.
[66] Y. Matsumura, M. Okumura, Y. Usami, K. Kagawa, H. Yamashita, M. Anpo, M. Haruta, Catal. Lett. 44 (1997) 189.